

Quantum-Classical Modeling of Nonlinear Pulse Propagation in a Dissolved Two-photon Active Chromophore

Alexander Baev,^{*,†} Pawel Salek,[‡] Faris Gel'mukhanov,[‡] and Hans Ågren[‡]

Institute for Lasers, Photonics and Biophotonics, State University of New York at Buffalo, Buffalo New York 14260-3000; Theoretical Chemistry, Roslagstullsbacken 15, Royal Institute of Technology, AlbaNova S-106 91 Stockholm, Sweden

Received: November 17, 2005; In Final Form: January 24, 2006

In the present work we outline the implications of a quantum-classical approach for modeling two-photon absorption of organic chromophores in solution. The approach joins many-photon absorption dynamic simulations with quantum chemical first principles calculations of corresponding excitation energies and transition matrix elements. Among a number of conclusions of the study, we highlight three: (i) The use of either short- or long-pulse excitation is demonstrated to switch the absorptive capacity of the nonlinear medium owing to enhancement of the nonlinear stepwise processes; (ii) The two-photon cross section strongly depends on the way in which the dephasing rate decays when the laser frequency is tuned off-resonant with the corresponding molecular transition; (iii) The results of the pulse propagation simulations based on electronic structure data obtained with a new Coulomb attenuated functional is shown to be in much better agreement with the experimental results than those based on data received with traditional density functionals.

1. Introduction

Novel organic materials have been of great interest during the past decade owing to a variety of exciting applications emerging at the interface between nonlinear optics, material science, biology, and nanotechnology.^{1,2} Reliable structure-to-property relationships have been established for a class of charge-transfer type compounds thanks to the progress in first principle quantum chemical calculations.³ In particular, there has been much interest in designing compounds with large two- and three-photon absorption cross sections for applications in biophotonics.² It has been shown, however, that comparison of *ab initio* results with numerous experimental data is in most cases justified only when the experimental results are obtained with a short-pulse (shorter than 100 fsec) excitation of the medium of interest. This is found to be at the expense of additional effects, such as stepwise many-photon absorption and absorption saturation processes, which manifest themselves when the exciting pulse is longer than the corresponding lifetimes of the molecular states. The authors address this problem using a more general modeling of nonlinear pulse propagation.^{4,5}

In this paper we use the previously advised combined quantum-classical modeling approach to nonlinear pulse propagation^{4,5} to explore pulse effects on two-photon absorption (TPA) capability, taking a dissolved 9,9-dialkylfluorene-based charge-transfer chromophore as demonstration example (abbreviated as AF240, see Figure 1). The purpose is to reveal key processes and properties for the all-over pulse propagation of a realistic system of experimental interest. We focus first on the underlying quantum chemical requirements of having a density functional with proper asymptotic dependence for charge-transfer excitations. With this as the basis, we go through

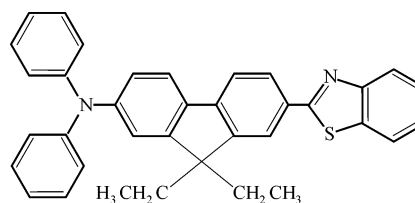


Figure 1. Chemical structure of AF240 molecule.

the conditions for modeling pulse propagation for both short and long pulses. The notion of a strong competition between coherent and incoherent, stepwise, processes is highlighted in the latter case, meaning that even at resonant conditions, stepwise TPA will contribute to the total effective TPA as measured in, e.g., a direct transmission experiment with long pulses. The stepwise processes will be enhanced in a way which is delicately dependent on how the dephasing rate decays when the laser frequency is detuned from the resonance with the molecular transition. The modeling adds up to a fairly complex picture, including stepwise and coherent processes where desaturation through excited-state absorption, intersystem crossings, and triplet absorption are generally important. The role of a solvent will be important, in particular, through the change of dephasing conditions, but also through reaction field, dielectric, enhancements.⁶

2. Electronic Structure Calculations

The nonlinear pulse propagation methodology employs a few-states model of the absorptive medium (in this paper), and it is supported by quantum chemical calculations of corresponding excitation energies and dipole moments. As shown earlier, few-step models are, in general, very applicable to two-photon absorption of charge-transfer species compared to sum-over state or full time-dependent solutions for the corresponding cross sections.⁷ A concern for larger charge-transfer species, such as AF240, is the long range behavior of common density func-

* Corresponding author email: abaev@buffalo.edu.

[†] State University of New York at Buffalo.

[‡] Royal Institute of Technology.

TABLE 1: Selected Relative Excitation Energies (ΔE , eV) and Dipole Moments (μ_i , A.U.) of the low-lying singlet states of AF240 (CAM-B3LYP/6-31G*)

μ_i	x	y	z	ΔE_{DFT}^a
S ₀ S ₀	0.6282	0.3803	0.1746	
S ₁ S ₁	-3.5494	-0.0309	-0.0382	
S ₁₀ S ₁₀	-4.1258	-0.0275	0.0108	
S ₁₁ S ₁₁	-1.6613	-0.1973	-0.1021	
S ₁₂ S ₁₂	-2.1384	-0.0215	-0.0066	
S ₀ S ₁	-4.0263	-0.0073	0.0406	3.58
S ₀ S ₁₀	-0.9724	-0.1274	-0.1468	5.08
S ₀ S ₁₁	0.2829	-0.0115	0.0019	5.29
S ₀ S ₁₂	-0.3141	0.2491	0.1642	5.53
S ₁ S ₁₀	4.9664	0.0162	-0.0177	
S ₁ S ₁₁	-1.3913	-0.1057	-0.0491	
S ₁ S ₁₂	0.5209	-0.0306	0.0392	

^a Absorption at the equilibrium ground-state geometry.

tionals. The B3LYP functional has an established successful history in many areas, however, its applications to charge-transfer systems do not belong on its list of most spectacular achievements. The reason is that the locality of the density functional theory is remedied only to a limited extent by the use of the nonlocal fractional Hartree–Fock exchange in B3LYP. It is known that long-distance interactions should decay as r^{-1} , but B3LYP accounts only for one-fifth of such interactions. CAM-B3LYP is an attempt to address this deficiency. It has the same fraction of Hartree–Fock exchange for short interactions as B3LYP, exchanging it smoothly to 65% for long-range ones. This smooth transition provides a universal functional with most of the good properties of B3LYP retained and much improved description of charge-transfer systems. Thus, another aim of our study was to compare the pulse propagation results based upon ab initio density functional theory (DFT) calculations with a traditional B3LYP functional with those obtained by using a new Coulomb attenuated functional CAM-B3LYP.⁹ The full time-dependent DFT TPA cross sections using CAM-B3LYP is discussed in ref 8.

The ground-state geometry of AF240 was optimized by making use of the Gaussian 98 code¹⁰ at the DFT B3LYP/6-31G* level. Ground to excited singlet state, absorption spectra were calculated by means of the linear response technique realized in the Dalton code¹¹ at the DFT B3LYP/6-31G* and CAM-B3LYP/6-31G* levels. Transition dipole moments between the excited singlet states were carried out by Dalton DFT quadratic response calculations at the B3LYP/6-31G* and CAM-B3LYP/6-31G* levels.

3. Results and Discussion

3.1. Extraction of Two-Photon Cross Sections from Nonlinear Transmittance Data. We simulated the nonlinear pulse propagation at several pump levels and two different pulse durations making use of our density matrix code presented in ref 12. The simulation sequence consists of obtaining linear transmittance by simulating propagation of pulse with low intensity, usually 1 GW/cm², and then in using the transmittance value to extract the off-resonant linear absorption coefficient. Afterward, the simulations are carried out for a broad range of intensities, usually from 10 MW/cm² to 100 GW/cm². The resulting values of the nonlinear transmittance are then employed to get the two-photon absorption cross section. Here, the quantum chemistry yields energies of molecular states and transition matrix elements which are needed to obtain the nonlinear polarization by solving coupled equations for the density matrix.

TABLE 2: Selected Relative Excitation Energies (ΔE , eV) and Dipole Moments (μ_i , A.U.) of the Low-lying Singlet States of AF240 (B3LYP/6-31G*)

μ_i	x	y	z	ΔE_{DFT}^a
S ₀ S ₀	0.7381	0.4505	0.0552	
S ₁ S ₁	7.1036	0.6461	0.1237	
S ₈ S ₈	-0.6764	0.0855	0.0058	
S ₉ S ₉	1.4551	0.9793	0.0132	
S ₁₀ S ₁₀	2.1333	0.6029	0.1468	
S ₀ S ₁	3.4557	0.0965	-0.0084	2.92
S ₀ S ₈	0.0202	-0.3271	0.1462	4.38
S ₀ S ₉	0.5284	-0.0119	0.0946	4.39
S ₀ S ₁₀	0.1112	-0.0016	-0.0257	4.55
S ₁ S ₈	-0.2936	0.0784	-0.0761	
S ₁ S ₉	-1.2098	0.3424	0.0788	
S ₁ S ₁₀	0.5334	0.4361	0.1218	

^a Absorption at the equilibrium ground-state geometry.**TABLE 3: Quenching Rates of Molecular States**

decay rate	value (sec ⁻¹)
Γ_{S_1}	0.49×10^9
Γ_{S_n}	1.00×10^{11}
Γ_{T_1}	1.00×10^6
Γ_{T_n}	1.00×10^{12}
γ_{ISC}	0.32×10^8

The results of the ab initio calculations of excitation energies and transition matrix elements, used in our simulations, are collected in Tables 1 and 2, and the quenching rates of molecular states are collected in Table 3. The impact of the CAM-B3LYP functional is most trivially seen on the excitation energies.⁸ When solvent effects and a correction for a finite basis set are taken into account one finds that the B3LYP functional underestimates them by 0.5 eV, while, in contrast, CAM-B3LYP, with these effects included, is able to reproduce the experimental number to within 0.1 eV.⁸

Plots of the nonlinear transmittance versus incident intensity were obtained as a result of the nonlinear pulse propagation simulations. To extract the cross sections from the nonlinear transmittance data, we derived expressions relating the TPA cross section to the nonlinear transmittance by solving the paraxial wave equation for the intensity of the exciting light

$$\frac{dI}{dz} = -N_0(\sigma^{(1)}I + \sigma^{(2)}I^2) \quad (1)$$

where N_0 is the concentration of the absorbing molecules, and $\sigma^{(1)}$ and $\sigma^{(2)}$ are linear and TPA cross sections, respectively. We first solved the wave eq 1, keeping only the term proportional to the square of the intensity in the right-hand side. This approximation is valid in the region of high intensities, where contributions to the total effective cross section from the TPA process dominates. The TPA cross section then reads as follows:

$$\sigma^{(2)} = \frac{1}{N_0 L} \cdot \frac{1/T - 1}{I_0} \quad (2)$$

It is, however, clear that linear absorption contributes to the total cross section estimated by means of eq 2. Therefore, to extract the “pure” TPA cross section from the nonlinear transmittance data, we solved the wave eq 1 keeping both right-hand side terms. The TPA cross section now reads

$$\sigma^{(2)} = \frac{\alpha_0 [\exp(-\alpha_0 L)/T - 1]}{N_0 I_0 [1 - \exp(-\alpha_0 L)]} \quad (3)$$

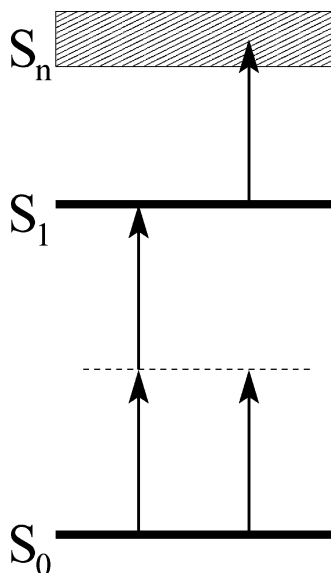


Figure 2. Energy level diagram showing the main TPA channels.

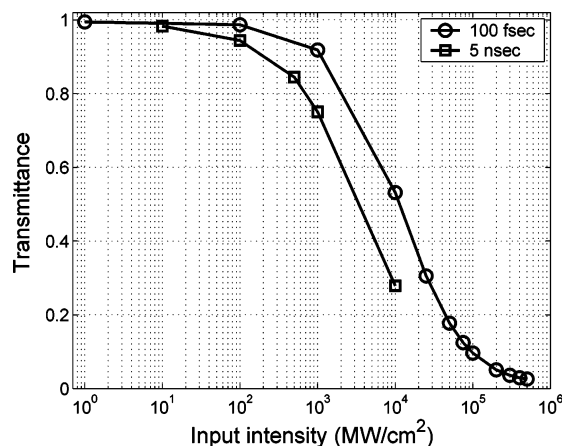


Figure 3. Nonlinear transmittance simulated with B3LYP data.

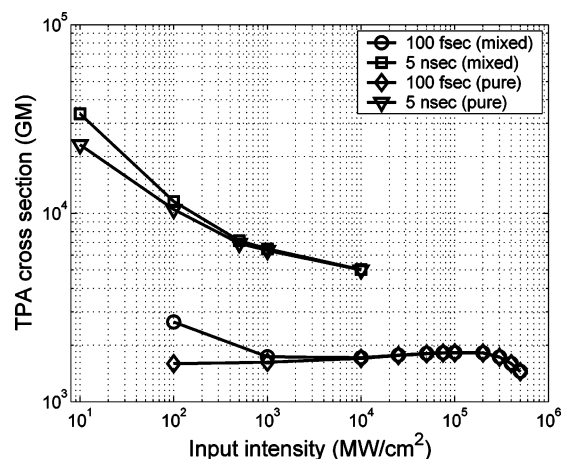


Figure 4. TPA cross sections simulated with B3LYP data.

where $\alpha_0 = N_0\sigma^{(1)}$ is the linear absorption coefficient estimated at the low intensity level.

The results of our simulations are presented in Figures 3–7. We simulated the propagation of a 100 fsec and of a 5 ns pulse through a 1 mm long cuvette filled with 0.02 M solution of AF240. The wavelength was chosen to fulfill the condition of the exact two-photon resonance between the ground and the first excited singlet states.

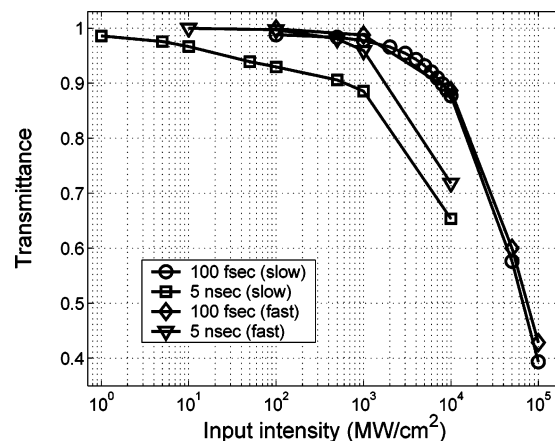


Figure 5. Nonlinear transmittance simulated with CAM-B3LYP data.

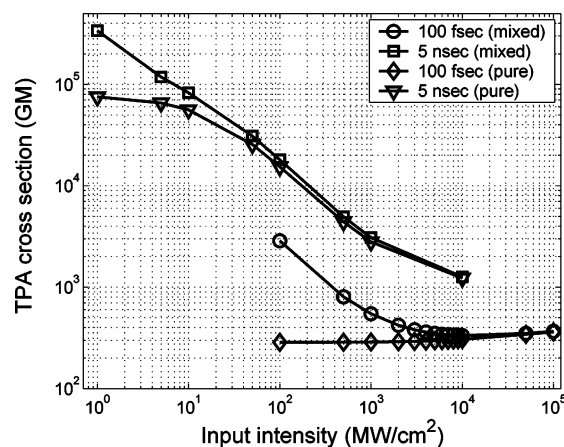


Figure 6. TPA cross sections simulated with CAM-B3LYP data under the slow-decay-of-dephasing-rate condition (3 orders of magnitude decay of the linear absorption intensity at the detuning of 1 eV).

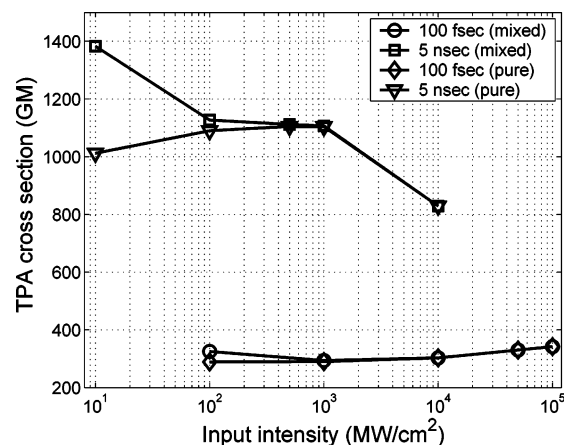


Figure 7. TPA cross sections simulated with CAM-B3LYP data under the fast-decay-of-dephasing-rate condition (5 orders of magnitude decay of the linear absorption intensity at the detuning of 1 eV).

The simulations based on B3LYP data show almost complete depletion of the pump when the intensity is higher than 100 GW/cm² (see Figure 3). The transmittance drops down faster for the long pulse, which is apparently due to the contribution of the stepwise processes going through either off-resonant one-photon or resonant two-photon population of the first excited electronic state with subsequent efficient resonant excited-state absorption. In contrast, the short pulse does not have time to populate the first excited state, which leads to a higher transmittance level compared to the long pulse. Indeed, extrac-

tion of TPA cross sections from the transmittance data reveals a much higher cross section value for the medium excited with the long pulse (see Figure 4). We want to stress here that the cross sections obtained by making use of eq 2 (noted “mixed” in the figure) differ from those obtained by making use of eq 3 (noted “pure” in the figure) in the region of low intensities. For the short pulse, the pure cross section almost does not change at all as the intensity changes, except for the region of very high intensities where the drop of the cross section can be attributed to saturation of the two-photon transition. At the same time, the mixed cross section curve goes up as the intensity decreases. The reason for this growth of the cross section is that the linear absorption, which we assumed to be negligible in eq 1, dominates the two-photon absorption in the region of low intensities. However, the picture changes in the case of the long pulses. As one can see, both pure and mixed cross sections decrease as the intensity increases, although this decrease is more pronounced for the mixed cross section curve. The reason for the decrease in the region of high intensities (>1 GW/cm²), where the mixed and pure curves coincide, can be explained by the effect of saturation. At the same time, the reason for the decrease of the pure cross section in the region of smaller intensities can be found in either an additional stepwise process, which is not accounted for in eq 1, or in one-photon saturation of the second step of the stepwise two-photon absorption. This second step is excited-state absorption, which has rather low saturation intensity because of the close-to-resonant conditions between the frequency of the transition to the higher excited state and the laser frequency.

Let us now pay attention to the nonlinear transmittance obtained as the result of simulations based on CAM-B3LYP data (see Figure 5). In the figure “slow” and “fast” denote transmittance obtained with different decay rates of coherence (see discussion in Section 3.2 below). Meanwhile, we have to note that the absolute values of transmittance are large compared to the B3LYP case presented in Figure 3. A high transmittance level means that the total effective absorption cross section is smaller in the CAM-B3LYP case compared to the B3LYP case. Indeed, comparison of the strongest two-photon absorption channels, which for charge-transfer molecules are always those related to the change of the dipole moment upon excitation¹³ ($[\mu_{S_1S_1} - \mu_{S_0S_0}]$, see Tables 1 and 2), shows that we must expect much stronger TPA in the B3LYP case. The difference between the transmittance levels obtained with the long- and short-pulse excitations again proves that the contribution of stepwise processes becomes important when the pulse is long. The extracted TPA cross sections presented in Figure 6 show the same trend as in the B3LYP case in the region of low and moderate intensities. However, we do not observe saturation of two-photon absorption in the region of high intensities. The reason for this is that the two-photon saturation intensity becomes higher when the TPA cross section decreases, which here is the case because we have about 1 order of magnitude difference between the TPA cross sections obtained in simulations with either B3LYP or CAM-B3LYP electronic structure data. It should also be noted that some slow increase of the TPA cross section with the increase of intensity, which can be observed in both cases (see Figures 4 and 6), is due to the processes of higher than second-order such as, for example, three-photon absorption which also includes two-photon absorption followed by excited-state absorption.

3.2. Effect on Two-Photon Absorption Cross Section of Non-Lorentzian Decay of Coherence. The decay rate of coherence is one of the medium parameters which controls the

manifestation of different absorption channels as they contribute to the effective absorption cross section. The decay rate of coherence consists of a term related to the decay rates of populations of the molecular states, and of another term related to the dephasing of the quantum oscillators:

$$\Gamma_{ij}(\omega) = \frac{1}{2}(\Gamma_{ii} + \Gamma_{jj}) + \gamma_{ij}(\omega) \quad (4)$$

Both terms lead to homogeneous broadening of the absorption lines. It appears that the second term, the so-called dephasing rate γ_{ij} , depends on the frequency of the exciting light, or, to be precise, on the detuning between the frequencies of light and molecular transition. Indeed, when the detuning is large, the absorption is very fast (duration of the process is inversely proportional to the detuning)¹⁴ and the molecule has not enough time to collide with molecules of the solvent. In this case, only the lifetime broadening contributes to the decay rate of coherence. In contrast, when the exciting light is in resonance with the molecular transition, the dephasing rate reaches its maximum value, which is measured to be between 0.01 and 0.1 eV for molecules in solutions. Making use of some recent experimental data on the far red wing of the absorption profile of AF240 in THF,¹⁵ we modeled the frequency dependence of the dephasing rate by an exponential function and used this model in our density matrix code.

The results of our simulations with two different decay parameters of the exponential and using a resonant value of the dephasing rate equal to 0.1 eV are presented in figures 5, 6, and 7. As one can see, the use of either slow (3 orders of magnitude drop in the intensity of linear absorption at the detuning of 1 eV) or fast (5 orders of magnitude drop in the intensity of linear absorption at the detuning of 1 eV) decay of the dephasing rate in simulations of the medium excited by the short pulse does not bring about any substantial difference in transmittance. The reason for this is clear: the main contribution to the cross section comes from the *resonant* coherent two-photon absorption when the short pulse is used. The pure TPA cross section curves coincide in this case (see Figures 6 and 7) which was expected. In contrast, the mixed TPA cross section curves behave differently: in the case of the fast decay of the dephasing rate this curve follows almost exactly the pure curve, while in the case of the slow decay the mixed TPA cross section increases as the intensity decreases. This fact proves once again that the contribution of the off-resonant linear absorption and, hence, of the stepwise two-photon absorption to the total effective cross section is important if the decay of the dephasing rate is relatively slow.

Let us now look closer at the results obtained in the simulations of the nonlinear propagation of the long pulse. First of all, the transmittance level appears to be higher when the decay of the dephasing rate is fast. This implies a lower TPA cross section compared to the case of the slow decay. Indeed, the difference between the TPA cross sections estimated at 1 GW/cm² is more than 3 times. Moreover, in the case of the fast decay, the pure TPA cross section grows up as the intensity increases (up to 1 GW/cm²), which is opposite to the case when the decay is slow. The reason for the different behavior of the TPA cross sections with change of intensity is the different appearance of the stepwise TPA process, which is suppressed in the case of the fast decay of the dephasing rate and boosted in the opposite case.

Finally, it is worthwhile to note that the fast, 5 orders of magnitude drop of linear absorption at the detuning of 1 eV, decay of the dephasing rate corresponds to the real experimental

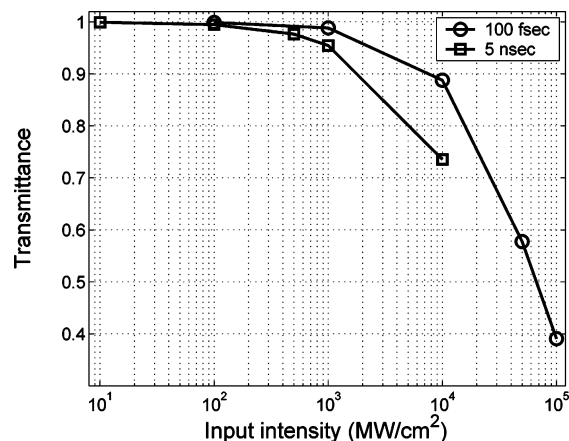


Figure 8. Nonlinear transmittance simulated with CAM-B3LYP data and the exact excited-state resonance.

situation reported in ref 15. In this case, the off-resonant linear absorption cross section measured at the half-a-resonant wavelength was reported to equal $2.85 \times 10^{-22} \text{ cm}^2$, whereas our simulations give $1.50 \times 10^{-22} \text{ cm}^2$.

3.3. Effect of Resonance in Excited-State Absorption on the Effective Two-Photon Absorption Cross Section. When the decay of the dephasing rate is fast and the detuning of the exciting light from resonant frequency of the transition between the first excited-state S_1 and higher excited-state S_n is larger than the resonant value of the dephasing rate (0.1 eV), the intensity of the $S_1 \rightarrow S_n$ absorption channel is greatly reduced. This means that the contributions of different stepwise processes, involving this excited-state absorption channel, to the effective two-photon absorption cross section are also reduced. This, in turn, leads to closer values of the effective TPA cross sections for the short and long pulses compared with the case of slow decay. Indeed, one can see from Figures 6 and 7 that at the intensity of 1 GW/cm^2 , the ratio between the effective TPA cross sections equals 9.7 in the case of slow decay and 3.8 in the case of fast decay. It follows, from our electronic structure calculations, that the higher excited-state S_n should be located at 5.37 eV for the exciting light to be in exact resonance with the $S_1 \rightarrow S_n$ transition (see Table 1). The energy of the S_{11} state appears to be close to this value. Since the calculated energy of the vertical transition is a little bit less than 5.37 eV, one could expect the frequency of the exciting light to be in resonance with a higher vibrational level of this S_{11} electronic state. Moreover, the calculated energy might even fit the exact resonance if we could find a way to improve the numerical accuracy of our ab initio calculations. To check the effect of having an exact resonance between the exciting light and $S_1 \rightarrow S_n$ transition on the effective TPA cross section, we performed simulations with the S_{11} energy shifted to 5.37 eV. The decay of the dephasing rate was then kept fast. The results are presented in Figures 8 and 9. The difference between the effective TPA cross sections was found to equal 4.1 in this case, compared to 3.8 for the case with detuning, something that proves that the contribution of the stepwise processes, such as excited-state absorption and two-step two-photon absorption, to the effective TPA cross section has increased. Figure 9 also shows a decrease of the effective absorption cross section with the increase of the light intensity when the pulse is long. The reason for this is saturation of the excited-state absorption channel $S_1 \rightarrow S_n$.

3.4. Effect of the Triplet-Triplet Absorption Channel on the Effective Two-Photon Absorption Cross Section. Al-

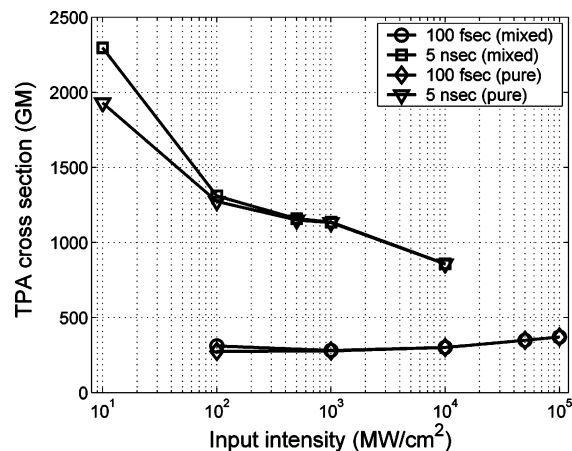


Figure 9. TPA cross sections simulated with CAM-B3LYP data under the fast-decay-of-dephasing-rate condition (5 orders of magnitude decay of the linear absorption intensity at the detuning of 1 eV) and the exact excited-state resonance.

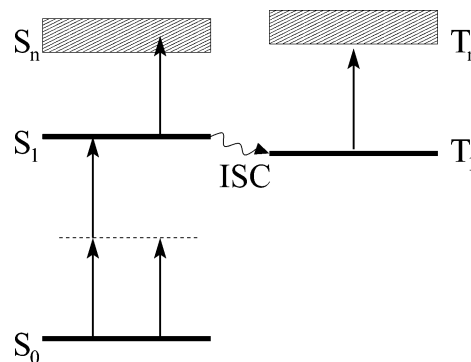


Figure 10. Energy level diagram featuring the triplet-triplet absorption channel.

though an exact resonance between the exciting light and the excited-state absorption channel $S_1 \rightarrow S_n$ brings about some increase of the effective TPA cross section in the case of a long pulse, the ratio between the effective TPA cross sections is still small in the case of the fast decay of the dephasing rate compared with the case of the slow decay. An additional absorption channel, contributing to the effective TPA cross section, is the intersystem crossing (ISC) with subsequent triplet-triplet absorption (see Figure 10). We simulated the nonlinear pulse propagation taking account of the triplet-triplet absorption channel and keeping the exact excited-state resonance. We have used experimental data for the triplet quantum yield (0.064), triplet-triplet absorption wavelength (760 nm), and the lifetime of the excited singlet state S_1 (2.03 ns).¹⁶ We should note here that the lifetime of 2.03 ns was used for the first excited singlet state in all simulation sets. The results are presented in Figures 11 and 12. Interestingly, at the intensity of 1 GW/cm^2 , the ratio between the effective TPA cross sections was found to equal 17. This means that even at a relatively low intersystem crossing rate the long pulse is being absorbed quite effectively, owing to almost exact resonance between the light frequency and the frequency of the triplet-triplet transition. We would like to stress here that, whereas the cross section dependencies for the short pulse behave exactly as the corresponding dependencies without the triplet-triplet absorption channel, the cross section curves for the long pulse behave differently. As one can see from Figure 12, the cross section for the long pulse increases as the intensity increases. This is a

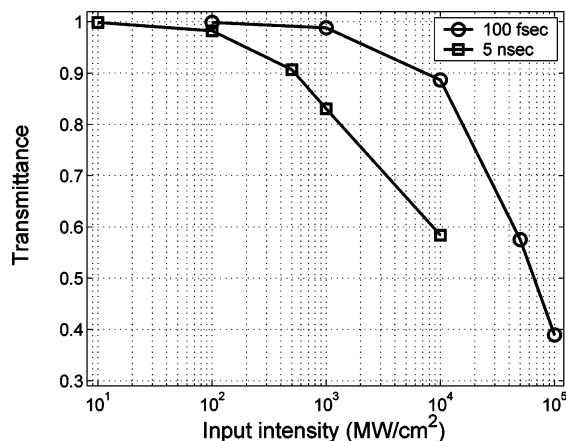


Figure 11. Nonlinear transmittance simulated with CAM-B3LYP data, the exact excited-state resonance, and triplet–triplet absorption channel.

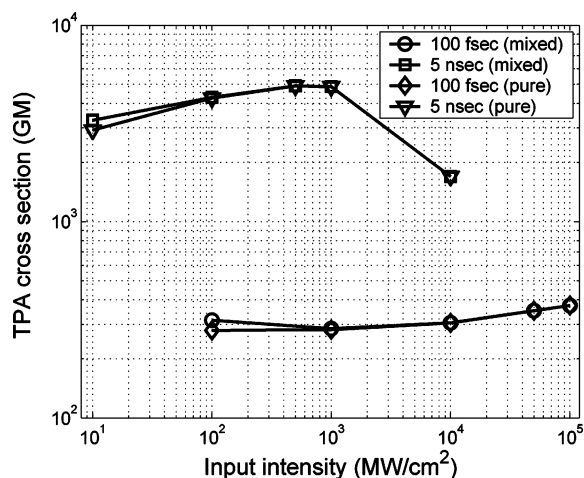


Figure 12. TPA cross sections simulated with CAM-B3LYP data under the fast-decay-of-dephasing-rate condition (5 orders of magnitude decay of the linear absorption intensity at the detuning of 1 eV), the exact excited-state resonance and triplet–triplet absorption channel.

manifestation of the triplet–triplet absorption channel which becomes more important when the intensity of the exciting light, or, equivalently, the two-photon pumped population of the first excited-state S_1 , increases. As one can see from the figure, this growth of the cross section gets slower with the increase of intensity and then turns to a plateau, followed by a decrease of the cross section as the intensity grows further. The saturation of the triplet–triplet channel is the reason for this behavior.

The qualitative and quantitative distinction between the intensity dependencies of the absorption cross sections (Figures 9 and 12) for the long pulse deserves a special comment. As it was mentioned above, the triplet–triplet channel starts to dominate in the effective two-photon absorption process when the intensity of the exciting light increases. To give the physical insight in this effect, let us give the simple estimation of the ratio of the effective absorption cross sections for $T_1 \rightarrow T_n$ and $S_1 \rightarrow S_n$ absorption channels:

$$\frac{\sigma_{T_1 \rightarrow T_n}^{(2)}}{\sigma_{S_1 \rightarrow S_n}^{(2)}} \approx \zeta \cdot \eta, \quad \zeta = \frac{\mu_{T_1 \rightarrow T_n}^2}{\mu_{S_1 \rightarrow S_n}^2} \cdot \frac{\tau}{\tau_{ISC}}, \quad \eta = \frac{1 + I/I_s^{S_1 \rightarrow S_n}}{1 + I/I_s^{T_1 \rightarrow T_n}} \sim \frac{I_s^{T_1 \rightarrow T_n}}{I_s^{S_1 \rightarrow S_n}} \quad (5)$$

where μ is the transition dipole moment and I_s is the saturation intensity of corresponding transitions. For pulse duration $\tau = 5$

ns and the ISC characteristic time $\tau_{ISC} = 32$ ns, we get $\zeta \approx 0.4$. The ratio of saturation intensities reads

$$\frac{I_s^{T_1 \rightarrow T_n}}{I_s^{S_1 \rightarrow S_n}} \approx \frac{\mu_{S_1 \rightarrow S_n}^2 \cdot \Gamma_{T_n}}{\mu_{T_1 \rightarrow T_n}^2 \cdot \Gamma_{S_n}} \quad (6)$$

where Γ_{S_n} and Γ_{T_n} are the quenching rates of corresponding molecular states. In our simulations we set the quenching rate of the triplet state T_n 1 order of magnitude larger than that of the singlet state S_n (Table 3). For large intensities we get $\eta \approx 4$, which gives us the ratio of the cross sections (5) equal to 1.6. Our simulations showed that, in agreement with estimations (3.4) and (3.4), the triplet–triplet channel is suppressed when the quenching rates of T_n and S_n states are set equal. In this case, the saturable $S_1 \rightarrow S_n$ excited-state absorption channel gives the main contribution to the effective TPA cross section, when the exciting pulse is long, as shown in Figure 9.

3.5. Accuracy Analysis. An attentive reader would certainly have noticed a large—more than 1 order of magnitude—discrepancy between the value of the TPA cross section obtained from simulations with the short pulse (300 GM) and the experimentally measured^{15,16} TPA cross section (17 GM). There are actually two main reasons for such a large disagreement. The first one is inhomogeneous vibrational broadening of the real spectra. In our derivation of the equations for the density matrix, we used the homogeneous decay rate of coherence, which would lead to a Lorentzian shape of the absorption profiles. This homogeneous decay rate usually measures 0.1 eV in solutions because of a large collisional dephasing rate as noted above. As a matter of fact, the real widths of the absorption profiles are much larger, up to 0.7 eV for the dissolved chromophores. One could describe an experimental absorption profile by a Gaussian distribution with a width parameter Δ , which varies around 0.3–0.4 eV. In this case, a simple analytical estimation of the resonant value of coherent one-step two-photon absorption would require to use Δ instead of conventional 0.1 eV in the denominator of the formula, which, in turn, would lead to an approximately 4 times drop of the value of the two-photon absorption cross section.¹³

The second reason is somewhat overestimated transition dipole moments. If we compared the resonant values of linear absorption cross section obtain in the experiment and estimated, with the aid of the computed transition dipole moments, we would see that the difference is almost 8 times and even the vibrational broadening correction (4 times) does not fully improve the situation. Thus, one could presume that the value of the transition dipole moment was overestimated $\sqrt{2} \approx 1.4$ times. In the case of the two-photon absorption cross section, this overestimation would result in as large as a 4 times difference. Combined with the vibrational broadening correction, it would give the factor of 16 and, hence, $300/16 = 19$ GM value of the two-photon absorption cross section, which is in the perfect agreement with the experimental value of 17 GM.

There are, of course, many other possible reasons of disagreement besides the two main mentioned above, for example self-focusing or self-defocusing of the laser beam, which we neglected having made use of paraxial approximation, which does not include the transverse inhomogeneity of the beam. However, the tradeoff between better accuracy and computational feasibility made us focus mainly on solving the system of the coupled algebraical and ordinary differential equations for the density matrix rather than on solving the wave equation without any approximations. In some limiting cases, when

simpler molecules are used and the prevalence of certain nonlinear processes is clear, the algorithms, such as the finite difference time domain (FDTD) method, could supposedly be more suitable.

4. Summary

We have studied the two-photon absorption capacity of a dissolved organic chromophore by means of nonlinear pulse propagation simulations in order to isolate and understand key mechanisms that are responsible for the all-over, measurable, multiphoton absorption. These simulations are combined with quantum chemistry technology for computing the basic excitation energies and cross sections. We have shown that the effective two-photon cross section strongly depends on the way in which the dephasing rate decays when the laser frequency is not in resonance with the corresponding molecular transition. We have confirmed our previous conclusions that the prominent difference between the TPA cross sections, obtained by direct transmittance measurements using long or short pulses, is due to the different stepwise processes, such as two-step two-photon absorption, excited-state absorption, and triplet–triplet absorption, of which the contributions to the effective TPA cross section are accentuated when the exciting pulse is long.

As shown in the present work, our all ab initio, classical-quantum, modeling approach lends itself easily for inclusion of measured photophysical parameters; thereby, giving the opportunity to isolate and study particular, rate limiting, sub-processes or properties in greater detail. We have compared the results based upon time-dependent density functional calculations using a new, asymptotically corrected, functional, and found that this gives more realistic values of excitation energies and cross sections compared to using traditional functionals. This considerably improves the prospects for accurate quantum treatments of larger charge transfer species with inherently high two-photon absorption cross sections. These opportunities and the flexibility of the quantum-classical approach give promise to combine with experimental work to provide even deeper insight into the nature of laser pulse propagation in nonlinear materials.

Acknowledgment. A.B. thanks the Swedish Research Council and the Swedish Foundation for International Cooperation in Research and Higher Education for a postdoctoral fellowship. We thank Dr. Paul Fleitz and co-workers at the Air Force Research Laboratory, Dayton, Ohio, for interesting

communication and for information on photophysical parameters which are used in this study. This work was supported by the Sensor-Protection project within the NanoTek program supported by the Swedish Defence Agencies (www.nanotek.se).

References and Notes

- (1) Reinhardt, B. A. *Photonics Sci. News* **1999**, 4, 21.
- (2) He, G. S.; Prasad, P. N. *Proc. SPIE-Int. Soc. Opt. Eng.* **2003**, No. 5211, 1.
- (3) Wang, C. K.; Macak, P.; Luo, Y.; Ågren, H. *J. Chem. Phys.* **2001**, 114, 9813.
- (4) Gel'mukhanov, F.; Baev, A.; Macak, P.; Luo, Y.; Ågren, H. *J. Opt. Soc. Am. B* **2002**, 19, 937.
- (5) Baev, A.; Gel'mukhanov, F.; Macak, P.; Luo, Y.; Ågren, H. *J. Chem. Phys.* **2002**, 117, 6214.
- (6) Frediani, L.; Rinkevicius, Z.; Ågren, H. *J. Chem. Phys.* **2005**, 122, 244104.
- (7) Cronstrand, P.; Luo, Y.; Ågren, H. *Chem. Phys. Lett.* **2002**, 352, 262.
- (8) Rudberg, E.; Salek, P.; Helgaker, T.; Ågren, H. *J. Chem. Phys.* **2005**, 123, 184108.
- (9) Yanai, T.; Tew, D. P.; Handy, N. C. *Chem. Phys. Lett.* **2004**, 393, 51.
- (10) Frisch, M. J.; Trucks, G. W.; Schlegel, H. B.; Scuseria, G. E.; Robb, M. A.; Cheeseman, J. R.; Zakrzewski, V. G., Jr.; Montgomery, J. A.; Stratmann, R. E.; Burant, J. C.; Dapprich, S.; Millam, J. M.; Daniels, A. D.; Kudin, K. N.; Strain, M. C.; Farkas, O.; Tomasi, J.; Barone, V.; Cossi, M.; Cammi, R.; Mennucci, B.; Pomelli, C.; Adamo, C.; Clifford, S.; Ochterski, J.; Petersson, G. A.; Ayala, P. Y.; Cui, Q.; Morokuma, K.; Malick, D. K.; Rabuck, A. D.; Raghavachari, K.; Foresman, J. B.; Cioslowski, J.; Ortiz, J. V.; Baboul, A. G.; Stefanov, B. B.; Liu, G.; Liashenko, A.; Piskorz, P.; Komaromi, I.; Gomperts, R.; Martin, R. L.; Fox, D. J.; Keith, A. L.; Lam, M. A.; Peng, C. Y.; Nanayakkara, A.; Challacombe, M.; Gill, P. M. W.; Johnson, B.; Wong, C. M. W.; Andres, J. L.; Gonzalez, C.; Head-Gordon, M.; Replogle, E. S.; Pople, J. A. *Gaussian 98, Revision A.9*, Gaussian Inc., Pittsburgh, PA **1998**. See <http://www.Gaussian.com>.
- (11) Helgaker, T.; Jensen, H. J. Aa.; Jørgensen, P.; Olsen, J.; Ruud, K.; Ågren, H.; Auer, A. A.; Bak, K. L.; Bakken, V.; Christiansen, O.; Coriani, S.; Dahle, P.; Dalskov, E. K.; Enevoldsen, T.; Fernandez, B.; Haettig, C.; Hald, K.; Halkier, A.; Heiberg, H.; Hetttema, H.; Jonsson, D.; Kirpekar, S.; Klopper, W.; Kobayashi, R.; Koch, H.; Mikkelsen, K. V.; Norman, P.; Pedersen, T. M.; Packer, M. J.; Rinkevicius, Z.; Rudberg, E.; Ruden, T. A.; Saek, P.; Sanchez, A.; Saue, T.; Sauer, S. P. A.; Schimmelpfennig, B.; Sylvester-Hvid, K. O.; Taylor, P. R.; Vahtras, O. *DALTON, a molecular electronic structure program*, Release 2.0 **2005**. See <http://www.kjemi.uio.no/software/dalton/dalton.html>.
- (12) Baev, A.; Gel'mukhanov, F.; Kimberg, V.; Ågren, H. *J. Phys. B: At., Mol. Opt. Phys.* **2003**, 36, 3761.
- (13) Baev, A.; Prasad, P. N.; Samoc, M. *J. Chem. Phys.* **2005**, 122, 224309.
- (14) Baev, A.; Salek, P.; Gel'mukhanov, F.; Ågren, H.; Naves de Brito, A.; Björneholm, O.; Svensson, S. *Chem. Phys.* **2003**, 289, 51.
- (15) McLean, D. G.; Sutherland, R. L.; Rogers, J. E.; Slagle, J. E.; Brant, M. C.; Fleitz, P. A. *Proc. SPIE-Int. Soc. Opt. Eng.* **2005**, 5934, 593401.
- (16) Sutherland, R. L.; Brant, M. C.; Heinrichs, J.; Rogers, J. E.; Slagle, J. E.; McLean, D. G.; Fleitz, P. A. *J. Opt. Soc. Am. B* **2005**, 22, 1939.